

Rossby Wave Breaking and Transport between the Tropics and Extratropics above the Subtropical Jet

CAMERON R. HOMEYER AND KENNETH P. BOWMAN

Department of Atmospheric Sciences, Texas A&M University, College Station, Texas

(Manuscript received 11 July 2012, in final form 14 September 2012)

ABSTRACT

Rossby wave breaking is an important mechanism for the two-way exchange of air between the tropical upper troposphere and lower stratosphere and the extratropical lower stratosphere. The authors present a 30-yr climatology (1981–2010) of anticyclonically and cyclonically sheared wave-breaking events along the boundary of the tropics in the 350–500-K potential temperature range from ECMWF Interim Re-Analysis (ERA-Interim). Lagrangian transport analyses show net equatorward transport from wave breaking near 380 K and poleward transport at altitudes below and above the 370–390-K layer. The finding of poleward transport at lower levels is in disagreement with previous studies and is shown to largely depend on the choice of tropical boundary. In addition, three distinct modes of transport for anticyclonic wave-breaking events are found near the tropical tropopause (380 K): poleward, equatorward, and symmetric. Transport associated with cyclonic wave-breaking events, however, is predominantly poleward. The three transport modes for anticyclonic wave breaking are associated with specific characteristics of the geometry of the mean flow. In particular, composite averages show that poleward transport is associated with a “split” subtropical jet where the jet on the upstream side of the breaking wave extends eastward and lies poleward and at lower altitudes of the subtropical jet on the downstream side, producing a substantial longitudinal overlap between the two jets. Equatorward transport is not associated with a split subtropical jet and is found immediately downstream of stationary anticyclones in the tropics, often associated with monsoon circulations. It is further shown that, in general, the transport direction of breaking waves is determined primarily by the relative positions of the jets.

1. Introduction

Rossby wave breaking is known to affect both the dynamics and chemistry of the upper troposphere and lower stratosphere (UTLS) (McIntyre and Palmer 1983). Previous studies have shown relationships with enhanced convection (Matthews and Kiladis 2000), cutoff lows and blocking anticyclones (Baray et al. 2003; Pelly and Hoskins 2003), hemispheric-scale climate patterns such as the North Atlantic Oscillation (NAO; Benedict et al. 2004), and stratosphere–troposphere exchange (STE; Scott and Cammas 2002). Understanding these dynamical and chemical impacts is important for simulating current and future climates. Two established methods for identifying Rossby wave breaking on potential temperature surfaces using fields of potential

vorticity (PV) or a similar dynamical quantity can be found in the literature. Postel and Hitchman (1999) provide a method for identifying Rossby wave-breaking events as meridional gradient reversals (folds) of PV. Wernli and Sprenger (2007) identify Rossby wave-breaking events as streamers and cutoff features of PV that, during most life cycles, evolve into meridional gradient reversals. Although these approaches use different wave-breaking diagnostics, analyses from the two methods are comparable (e.g., Postel and Hitchman 1999; Wernli and Sprenger 2007; Martius et al. 2007; Song et al. 2011). In addition, analyses of breaking Rossby waves have typically included the separation of events by their evolution—namely, whether they occur in areas of anticyclonic or cyclonic shear and whether they break predominantly poleward or equatorward. Thorncroft et al. (1993) propose the classification of equatorward breaking waves as type LC1 (anticyclonic) or LC2 (cyclonic). Peters and Waugh (1996) similarly classify poleward breaking waves as type P1 (cyclonic) or P2 (anticyclonic). All four types have been studied

Corresponding author address: Cameron Homeyer, National Center for Atmospheric Research, 1850 Table Mesa Dr., P.O. Box 3000, Boulder, CO 80305.
E-mail: chomeyer@ucar.edu

recently in regard to their meridional fluxes of Rossby wave activity (e.g., Gabriel and Peters 2008; Ndarama and Waugh 2011).

Rossby wave breaking is an important mechanism for horizontal transport between the tropical UTLS and extratropical LS. Recent studies have examined the characteristics of individual Rossby wave-breaking events with predominantly poleward transport above the subtropical jet, often on the 380-K potential temperature surface (e.g., Newman and Schoeberl 1995; Vaughan and Timmis 1998; O'Connor et al. 1999; Bradshaw et al. 2002; Pan et al. 2009; Homeyer et al. 2011), which is conventionally taken to be the level of the tropopause in the deep tropics (Holton et al. 1995). Pan et al. (2009) label these poleward transport events as “tropospheric intrusions.” Rossby wave breaking, however, is known to be a two-way transport mechanism and there have also been studies focused on intrusions of extratropical LS air into the tropical UT (e.g., Waugh and Polvani 2000; Waugh 2005; Konopka et al. 2010; Ploeger et al. 2012). As discussed in Pan et al. (2009), Rossby wave breaking has not been studied extensively in the 370–400-K potential temperature range where tropospheric intrusions have been observed. Previous studies have focused largely on wave breaking at the tropopause in the 320–360-K potential temperature range, which is usually below and poleward of the subtropical jet. The frequency of Rossby wave breaking near the tropopause at 350 K has been shown to peak from late spring into summer (e.g., Postel and Hitchman 1999; Hitchman and Huesmann 2007; Song et al. 2011).

The irreversible transport properties of wave-breaking events between the troposphere and stratosphere are not entirely understood. Scott and Cammas (2002) illustrate that the dependence of mixing (or transport) intensity along the tropopause in the Northern Hemisphere reaches a maximum over the Atlantic region, while a secondary maximum is observed over the Pacific region, which is consistent with previous climatologies of wave-breaking frequency. The analyses presented in Scott and Cammas (2002) relate the observed maximum in mixing over the Atlantic to the dual meridional structure of the jet there. There are also several studies of isentropic transport and mixing between the tropics and extratropics, which is dominated by Rossby wave breaking (e.g., Chen et al. 1994; Waugh 1996; Dethof et al. 2000; Seo and Bowman 2001; Jing et al. 2005; Nakamura 2007). As is true for investigations of Rossby wave-breaking frequency, isentropic transport studies have largely been limited to potential temperature levels at or below 360 K and above 500 K. It is evident from these analyses, however, that quantitative estimates of transport are sensitive to the dynamical representation of the

tropopause and collectively show net stratosphere-to-troposphere transport at potential temperature levels at or below 350 K.

Transport calculations depend on how the boundaries between domains of interest are defined. Because of its quasi-conservative nature, potential vorticity is commonly used to define the boundary between the tropics and extratropics, or between the stratosphere and troposphere, but as we will show quantitative transport calculations can depend strongly on the value of the PV surface used to define the boundary. For example, estimates of stratosphere–troposphere exchange in the extratropics depend on whether a PV surface or the lapse-rate tropopause is used as the boundary between the troposphere and stratosphere (e.g., Pan et al. 2004; Hegglin et al. 2009).

As an example of the sensitivity of transport estimates to the definition of the troposphere–stratosphere boundary, Fig. 1 shows the late stages of an anticyclonic Rossby wave-breaking event on the 350-K surface that injects tropical air into the extratropics. Three PV isopleths are highlighted in black [3, 4, and 5 potential vorticity units (PVU), where $1 \text{ PVU} = 10^{-6} \text{ K m}^2 \text{ kg}^{-1} \text{ s}^{-1}$]. Away from the wave-breaking region, all three contours lie close together, indicating a sharp PV gradient between the tropics and extratropics. In the wave-breaking region, however, their behavior is quite different. The 3-PVU contour remains entirely within the tropics; it is not stretched or folded during the event. In contrast, the 4- and 5-PVU contours show large stretching and folding in the meridional direction (Fig. 1a). As the breaking wave evolves and separates from the tropical reservoir downstream, the 4- and 5-PVU contours show that a substantial volume of air from the boundary region has been drawn into the extratropical LS (Fig. 1b). At 2 and 4 days later (Figs. 1c and 1d), the air mass has been further stretched and mixed into the extratropical LS, as is evidenced by the decreasing area enclosed by the 4- and 5-PVU contours. In this example, using 3 PVU as the troposphere–stratosphere boundary would lead one to infer that no transport had taken place. Using the 4- or 5-PVU contour as the boundary, on the other hand, would lead to inference of poleward transport, but at significantly different rates. Therefore, the choice of boundary can have a critical impact on the estimation of transport and the net annual transport direction (troposphere to stratosphere or stratosphere to troposphere). Section 2b will show that approximately 4 PVU provides a good representation of the boundary between tropics and extratropics at 350 K and that the PV value of the boundary depends on altitude.

Several modeling studies have examined the dependence of wave-breaking evolution on the structure of the

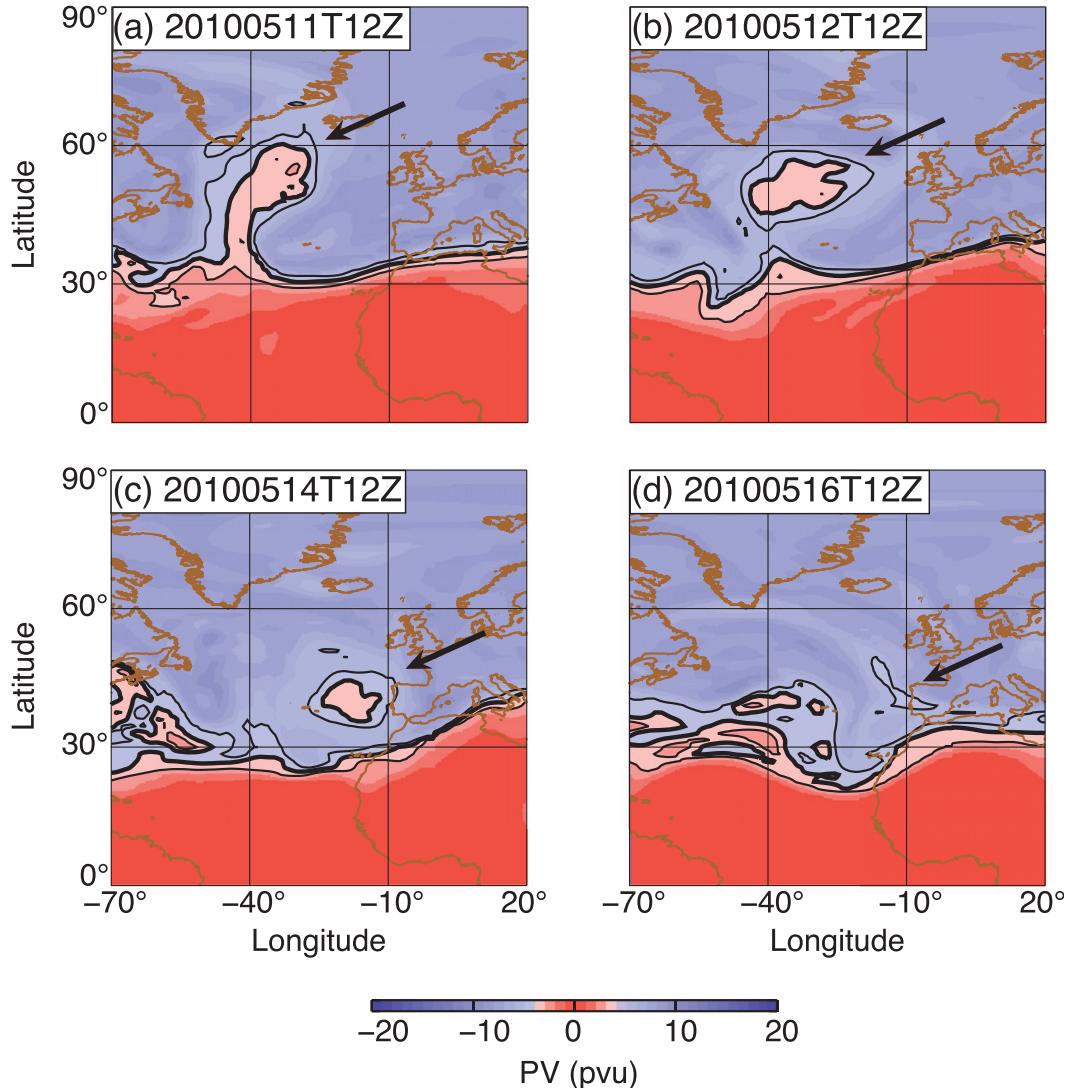


FIG. 1. Evolution of a Rossby wave–breaking event on the 350-K potential temperature surface from the ERA-Interim valid 1200 UTC (a) 11 May, (b) 12 May, (c) 14 May, and (d) 16 May 2010. Red colors represent $|PV| < 4$ PVU (tropical air); the black contours represent 3, 4 (thick), and 5 PVU. Black arrows identify the transported air mass at each analysis time.

Downloaded from http://journals.ametsoc.org/jas/article-pdf/70/2/607/3814304/jas-d-12-0098_1.pdf by guest on 28 October 2020

jet. The primary direction of breaking Rossby waves is known to depend on asymmetries of the mean flow in either the zonal or meridional direction and on the distance to the nearest critical line in the meridional direction (e.g., Nakamura and Plumb 1994; Peters and Waugh 1996). Although these model studies illustrate that idealized jet structures can produce wave breaking in either or both directions, the dependence of wave-breaking direction on the mean flow in observations of the UTLS is not known. Previous observational studies suggest that poleward wave-breaking events above the subtropical jet may be associated with a double-jet structure in the meridional direction (e.g., Peters and

Waugh 2003; Pan et al. 2009; Homeyer et al. 2011). Analysis of individual events show that the double-jet structure can be the result of the subtropical jet splitting, migrating poleward on the upstream side of the wave-breaking event and overrunning the equatorward subtropical jet downstream.

The goal of this study is to characterize the occurrence and transport properties of Rossby wave breaking between the tropics and extratropics above the subtropical jet. We present a climatology of wave-breaking events from European Centre for Medium-Range Weather Forecasts (ECMWF) Interim Re-Analysis (ERA-Interim) in the 350–500-K potential temperature range, which is

a layer spanning the tropical UTLS and extratropical LS. We use a seasonally varying definition of the boundary between tropics and extratropics (troposphere and stratosphere at some levels) for wave-breaking identification. For transport identification, we employ a Lagrangian method similar to that of Seo and Bowman (2001) to represent mixing of tropical (extratropical) air into the extratropics (tropics). Composite mean dynamical states for wave-breaking events are also shown to illustrate the dependence of transport direction on the mean flow.

2. Data and methods

a. ERA-Interim data

To compute the Rossby wave-breaking climatology we use 30 yr (1981–2010) of the ERA-Interim global atmospheric product (Dee et al. 2011). Reanalyses are provided daily at 0000, 0600, 1200, and 1800 UTC on a horizontal Gaussian grid with a longitude–latitude resolution of $0.75^\circ \times \sim 0.75^\circ$ (~ 80 km) and 37 unevenly spaced pressure levels in the vertical. For all of the analyses presented here, meteorological parameters are interpolated linearly to a regular $1.5^\circ \times 1.5^\circ$ grid in the horizontal and to nine potential temperature surfaces: 350, 360, 370, 380, 390, 400, 420, 450, and 500 K.

b. Tropical boundary definition

Because the goal of this study is to characterize Rossby wave breaking and isentropic transport above the subtropical jet between the tropical UTLS and the extratropical LS, an appropriate definition of the boundary between the tropics and extratropics is required. In this study, we use the lapse-rate tropopause to identify the tropical–extratropical boundary. The tropopause is found at high altitudes in the tropics (15–17 km) and at low altitudes in the extratropics (<12 km), as is evidenced by a clear bimodal frequency distribution in previous studies [e.g., Seidel and Randel (2007), their Fig. 1, or Birner (2010), their Fig. 5]. The transition between the two regions usually lies within a narrow latitude range near the subtropical jet. This sharp jump in tropopause height is referred to as the “tropopause break” (e.g., Randel et al. 2007; Castanheira and Gimeno 2011) and can often be observed indirectly using column ozone measurements (Hudson et al. 2003). We use the location of the break as the time-varying boundary between the tropical tropospheric air on the equatorward side of the jet and extratropical stratospheric air on the poleward side of the jet. The histogram of tropopause heights from the ERA-Interim for the entire 30-yr period and individual analysis times is bimodal with a distinct

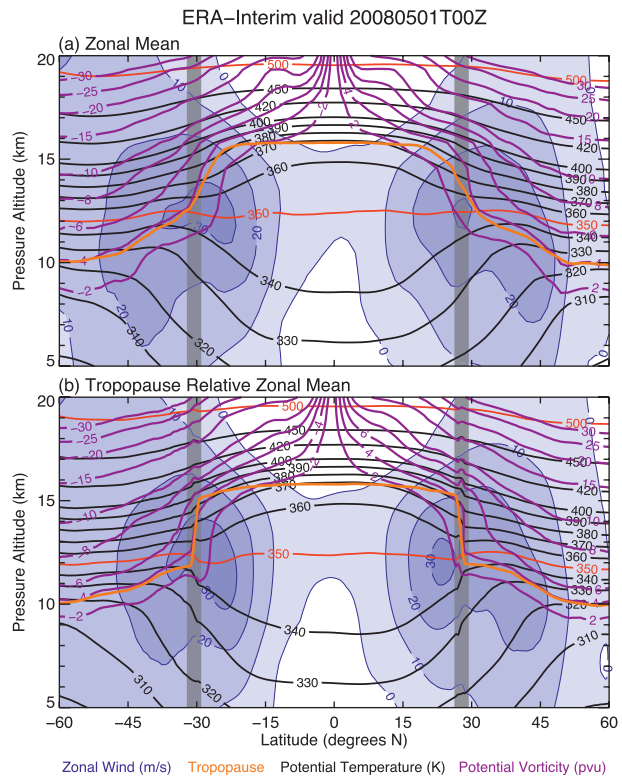


FIG. 2. Zonal mean zonal wind ($m s^{-1}$, color fill), potential temperature (K, black and red lines), potential vorticity (purple lines), and tropopause altitude (orange line) for (a) the pressure altitude vertical coordinate and (b) the tropopause-relative vertical and tropopause-break-relative horizontal coordinates from the ERA-Interim valid at 0000 UTC 1 May 2008. The mean latitude of the tropopause break, taken as the global 13-km tropopause altitude contour, is shown as the thick gray vertical lines in each hemisphere. The width of these gray lines corresponds to tropopause break latitude $\pm 1.5^\circ$ (the reanalysis horizontal grid resolution).

minimum at pressure altitudes near 13 km located between the tropical and extratropical modes (not shown). For this analysis, we identify the tropopause break in each hemisphere as the location of the 13-km tropopause altitude contour that extends completely around the globe (360° of longitude). Because the tropopause is uniformly higher than 13 km in the deep tropics and lower than 13 km in high latitudes, this contour is guaranteed to exist. The latitude of the contour can vary significantly for a given analysis time.

An example of the observed sharpness of the troposphere–stratosphere transition across the tropopause break is given in Fig. 2. The tropopause is calculated by applying the World Meteorological Organization (WMO) definition (World Meteorological Organization 1957) to the ERA-Interim data on the regular 1.5° horizontal grid following the algorithm outlined in

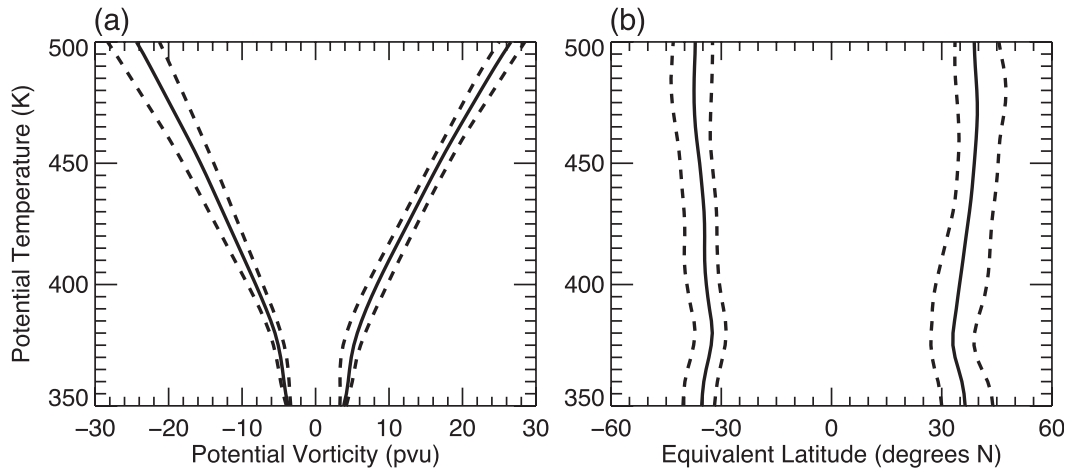


FIG. 3. ERA-Interim annual-mean (solid lines), -minimum, and -maximum (dashed lines) (a) potential vorticity and (b) equivalent latitude at the tropopause break ($Z_{\text{trop}} = 13$ km) from 30-yr climatological monthly means (1981–2010). Profiles of negative magnitudes represent the Southern Hemisphere and positive magnitudes the Northern Hemisphere.

Homeyer et al. (2010). Figure 2a shows conventional Eulerian zonal-mean meteorological fields from the ERA-Interim at 0000 UTC on 1 May 2008. Figure 2b shows the same analysis in a coordinate system that is averaged relative to the tropopause in altitude and relative to the tropopause break in latitude (the 13-km altitude contour) (e.g., Pan and Munchak 2011). The red contours of potential temperature in each section show the bounds of the wave-breaking layer analyzed in this study (350–500 K). The small-scale undulations in potential temperature and PV in Fig. 2b within the gray-shaded columns, which are 3° wide (two gridpoint intervals), are artifacts resulting from the relative-altitude averaging in regions where the altitude of the tropopause is highly variable. This tropopause-relative zonal-mean view illustrates the sharpness of the boundary between the troposphere and stratosphere along the subtropical jet. This cannot be seen in a conventional zonal mean because of zonal variation of the latitude of the tropopause break (Fig. 2a).

Potential temperature surfaces above about 380 K generally lie above the tropical tropopause. Analyses of the location of the maximum meridional PV gradient show that it coincides with the tropopause break in the 350–370-K potential temperature range and extends into the LS (e.g., Kunz et al. 2011). This suggests that the tropopause break is also a useful choice for the tropical–extratropical boundary in the lower stratosphere, and in this analysis we assume that the boundary at levels above 380 K lies at the same location as the tropopause break.

The jump in the lapse-rate tropopause at the subtropical jet provides a natural boundary between the

tropics and extratropics in the layer above the jet, but wave-breaking diagnostics are more meaningfully computed using a conserved quantity such as PV. Therefore, we calculate climatological values of PV along the 13-km tropopause height contour to identify a PV value that best represents the location of the tropopause break. Figure 3a shows the annual-mean PV along the tropopause break as a function of altitude (solid line). The dashed lines indicate the annual range of the climatological monthly-mean values. Note the natural increase of PV as the static stability increases with altitude. At all altitudes and in both hemispheres, the annual variation of PV along the tropopause break is small (± 0.5 –1.5 PVU, depending on altitude). Previous studies have often chosen PV values near ± 2 PVU as the tropical–extratropical boundary in the 350–370-K potential temperature range. We find that the average PV along the tropopause break in that layer is closer to ± 4 -PVU and the ± 2 -PVU isopleths usually lie within the tropics (see also Fig. 2b). These differences in the location of the tropical boundary have significant impacts on estimates of the direction and magnitude of transport.

To allow for easier comparisons between results at different levels, we use PV-based equivalent-latitude coordinates rather than PV itself (e.g., Butchart and Remsberg 1986). Equivalent latitude is a quasi-conservative PV-based meridional coordinate that effectively removes zonal variability due to large-scale waves. For a given PV value q_0 , the equivalent latitude ϕ_e is defined as the latitude of the boundary of a symmetric polar cap whose area is equal to the area of all locations with $q > q_0$. There is a one-to-one correspondence between PV and equivalent latitude. In physical terms, equivalent latitude tells you

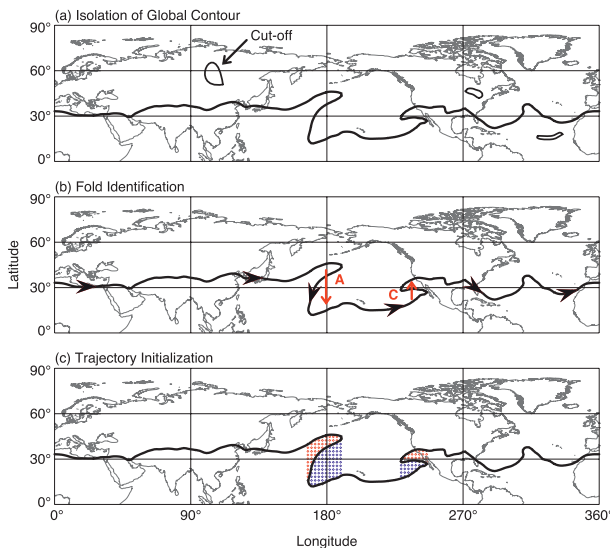


FIG. 4. An illustration of the identification process for wave-breaking events described in section 2c.

the latitude that an air parcel would have if all of the parcels on an isentropic surface were rearranged to be zonally symmetric and to have PV monotonic in latitude. Figure 3b shows the annual mean and annual range of climatological monthly-mean equivalent latitude along the tropopause break.

c. Wave-breaking identification

Once an appropriate PV value for the tropical boundary has been chosen, Fig. 4 illustrates the necessary steps to identify a continuous boundary in an instantaneous analysis and to characterize wave-breaking events. We identify Rossby wave-breaking events using a method similar to that outlined in Postel and Hitchman (1999). For a given potential temperature surface, wave breaking exists at a particular longitude if there is a significant reversal in the meridional gradient of PV or equivalent latitude. To require that gradient reversals involve deep tropical and extratropical air masses, Postel and Hitchman (1999) consider a reversal of at least ± 0.5 PVU relative to the PV boundary used as evidence of Rossby wave breaking. Comparisons with the PV reversal criteria in Postel and Hitchman (1999) at 350 K reveal that an equivalent-latitude reversal of $\pm 2.5^\circ$ relative to the boundary is comparable. Although not shown, the distribution of equivalent-latitude reversals for identified wave-breaking events in this study has a sharp peak at $\pm 5^\circ$ and a long tail to larger reversals, which suggests that the chosen threshold sufficiently captures nearly all potential wave-breaking features. Less than 8% of wave-breaking events at any surface analyzed in this study have gradient reversals less than $\pm 5^\circ$. It should be emphasized here that the use of

equivalent latitude to identify dynamic contour folds is exactly equivalent to the identification with a corresponding PV value. Small differences between the results given from the methods used in Postel and Hitchman (1999) and this study may occur because of the choice of the 2.5° threshold in equivalent-latitude coordinates instead of the 0.5-PVU threshold in PV space. Figure 3b shows that the annual cycle of equivalent latitude at the tropopause break is large (10° – 15°) because of the seasonality of the meridional location of the subtropical jet and tropopause break. To account for the annual cycle of equivalent latitude at the tropopause break, we use climatological monthly-mean values of ϕ_e to define the contours used for wave-breaking analysis.

Figure 4a illustrates the identification of a continuous tropical boundary for identifying gradient reversals (folds). At any given analysis time, there may be cutoff regions of tropical air masses within the extratropical reservoir (or vice versa). These cutoffs may be residual evidence of previous wave-breaking events. To identify active Rossby wave-breaking events between tropical and extratropical air masses and ignore cutoff regions, we first identify globe-circling contours of the appropriate equivalent-latitude value in each hemisphere. Each global contour is then searched for regions of meridional folding. Following Postel and Hitchman (1999), if the meridional gradient reversal criteria within a folded region are satisfied for at least 10° of consecutive longitude, the fold is tagged as a Rossby wave-breaking region. This 10° longitude threshold is used to exclude folds that result from processes that take place at scales much smaller than Rossby waves. The magnitude of the gradient reversal at each longitude, the contour segments of the equatorward and poleward boundaries of the folded region, and the areas of the tropical and extratropical air masses are saved for further analysis.

Figure 4b illustrates the classification of wave-breaking evolution: anticyclonic or cyclonic. In previous studies, anticyclonically and cyclonically sheared breaking waves have been separated by the local downstream longitudinal PV gradient and/or the meridional component of the wave activity flux (e.g., Esler and Haynes 1999; Gabriel and Peters 2008; Ndarana and Waugh 2011). In this study, we use a novel approach to separate anticyclonic and cyclonic wave breaking by the direction of the meridional fold in each global equivalent-latitude contour. In the example in Fig. 4b, an anticyclonically sheared breaking wave is identified over the central Pacific and a cyclonically sheared breaking wave is identified over the eastern Pacific.

The wave-breaking signatures detected in each instantaneous field are objectively linked with succeeding

times to identify full wave-breaking life cycles. We consider wave-breaking events to be those that are identified for at least three consecutive analysis times (18 h) and 1) if anticyclonic, have a minimum eastward propagation of 1.5° and a maximum eastward propagation of 15° , and 2) if cyclonic, have a maximum zonal propagation in either direction of 15° . Subjective analyses suggest that requiring a minimum wave-breaking life cycle is necessary to avoid the identification of small, short-lived folds in the dynamical boundary that do not exhibit characteristics consistent with irreversible Rossby wave breaking. Minimum propagation distances are used for anticyclonic wave-breaking events to avoid overidentification of stationary dynamical features such as monsoon circulations. Maximum propagation distances between analysis times are used to correctly associate regional wave-breaking signatures between analysis times. Once linked, the wave-breaking event life cycles are used for characterization and transport analyses.

Previous studies of isentropic transport between the tropics and extratropics in the 350–500-K potential temperature layer are calculated using Lagrangian methods initialized at regular time intervals. In this study, we provide a new event-based transport analysis to avoid over- or underidentification of responsible transport processes that occur over varying time scales. We identify transport for each individual Rossby wave-breaking event by using forward trajectories initialized in the tropical and extratropical air masses of the identified fold (red and blue particles in Fig. 4c). At the final analysis time of each event, particles are initialized at a longitude–latitude resolution of $0.5^\circ \times 0.5^\circ$ and advected forward isentropically for 10 days. If particles in the tropical (extratropical) air mass gain (lose) 5° of equivalent latitude and are within regions of extratropical (tropical) tropopause heights [below (above) 13 km] 10 days downstream, they are considered to be irreversibly transported (mixed). Quantitatively, if the initial area of tropical air covered by red particles in a wave-breaking event is A , the area covered by red particles that meet the above criteria for irreversible transport is A_i , while the particles that do not meet the criteria for irreversible transport have area A_r , so $A = A_i + A_r$. The fraction of the initial area that is irreversibly transported poleward is $f_i^P = A_i/A$. Similarly, for the other side of the PV fold (blue particles), the fraction of the extratropical air that is irreversibly transported equatorward is denoted f_i^E .

Although the transport calculations depend upon the choice of equivalent-latitude change, inspection of many events suggests that a 10-day equivalent-latitude change of 5° is appropriate for the ERA-Interim dataset. Such

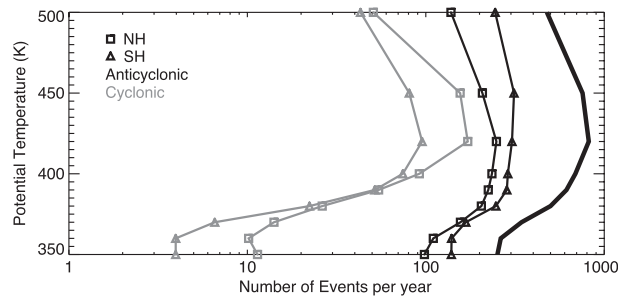


FIG. 5. The number of wave-breaking events identified in the ERA-Interim from 1981 to 2010 as a function of potential temperature. Symbols illustrate the potential temperature surfaces used. The gray symbol-marked lines represent the number of cyclonically sheared events and the black symbol-marked lines anticyclonic events. Square symbols are Northern Hemisphere events and triangle symbols are Southern Hemisphere events. The thick black line is the total of all four profiles.

a threshold identifies air that is transported a significant distance in PV coordinates from its original reservoir. In addition, previous studies have shown that transport and mixing for a given event using contour advection techniques generally takes place within the first 7 days of its life cycle (e.g., Dethof et al. 2000). For that reason, the transport estimates presented in this analysis are expected to be comparable to those from previous studies. Trajectory analyses of the observed wave-breaking events follow the methods given in Bowman et al. (2007). In this study, higher-resolution, three-dimensional ERA-Interim wind fields are used with the TRAJ3D trajectory model of Bowman (1993) and Bowman and Carrie (2002).

3. Results

a. Frequency, seasonality, and transport

The Rossby wave-breaking identification techniques described in section 2c were applied to 30 yr of ERA-Interim (1981–2010). The total number of events that occurred during the analysis period is plotted in Fig. 5 as a function of potential temperature. The fewest Rossby wave-breaking events are found at the lowest potential temperature levels (350–360 K, near the core of the subtropical jet). The frequency increases with altitude up to a pronounced maximum at 420 K. The general behavior is consistent across hemispheres and wave-breaking sense (cyclonic or anticyclonic). Anticyclonically sheared wave-breaking events dominate in both hemispheres and at all altitudes. Anticyclonic events constitute a greater fraction of the total events in the Southern Hemisphere than in the Northern Hemisphere at all altitudes, while the opposite is true for cyclonic

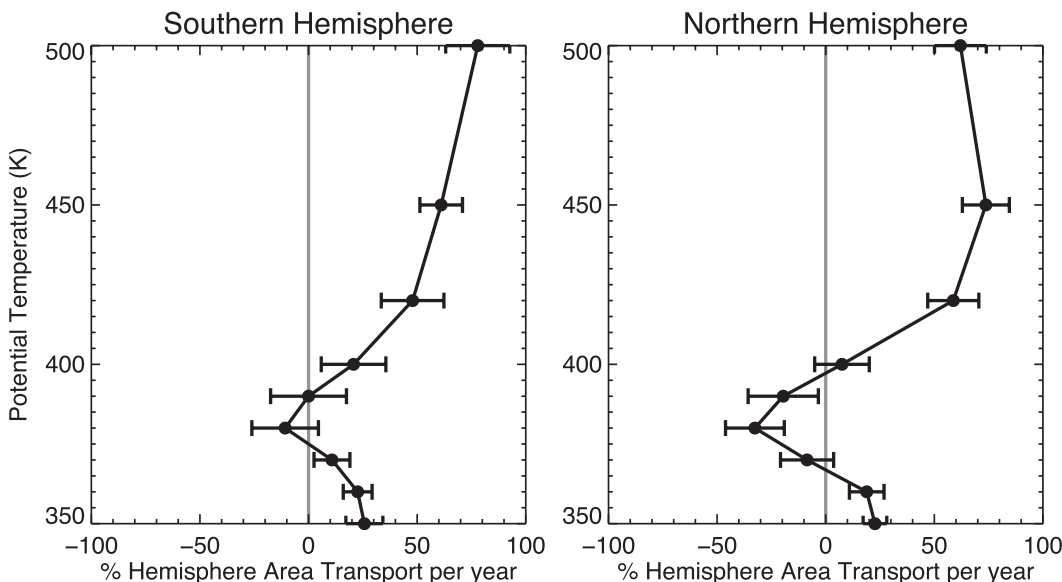


FIG. 6. Net annual Rossby wave-breaking transport as a function of potential temperature for (left) the Southern Hemisphere and (right) the Northern Hemisphere. In each plot, the black line is the mean and error bars are the standard deviation. Transport magnitudes are shown as the percentage of the area of one hemisphere. Negative values represent net transport into the tropics and positive values into the extratropics.

events. In addition, cyclonically sheared wave-breaking events are nearly absent at the lowest altitudes (fewer than about 10 yr^{-1} in each hemisphere), increase by an order of magnitude with increasing altitude from 360 to 420 K, and then decrease at higher levels. This variation contributes to the observed peak in total wave-breaking events at 420 K. Anticyclonic events increase rapidly from 360 to 380 K but have nearly constant frequencies above 380 K. Annual cycles of wave-breaking frequency in the 350–400-K potential temperature range (not shown) are comparable to results from previous studies at 350 K, which show a strong peak in the summer of each hemisphere (e.g., Postel and Hitchman 1999). There is no observed annual cycle at 420 K in this analysis, while the annual cycle becomes strong again at 500 K, but is shifted 6 months relative to the lower altitudes (a winter peak). This behavior at 500 K is consistent with the occurrence of mean easterly winds at this level during summer, which inhibit Rossby wave propagation altogether.

Net annual Rossby wave-breaking transport estimates from trajectory calculations of all events are shown in Fig. 6 as a function of potential temperature. Transport magnitudes are shown as the percentage of the area of one hemisphere with error bars (plus/minus one standard deviation) illustrating the interannual variability. The remaining discussion refers to transport into the tropics as equatorward and transport into the extratropics as poleward. For both hemispheres, net transport

is poleward except from 370–390 K in the Northern Hemisphere and 380–390 K in the Southern Hemisphere with a sharp peak in net equatorward transport at 380 K. Net poleward transport aloft is comparable to previous studies at 500 K (e.g., Waugh 1996). Poleward transport below 370 K, however, disagrees with previous studies of isentropic transport.

On the basis of Fig. 6, and other analyses to be presented later, the potential temperature levels can be grouped into four distinct layers: 350–360, 370–400, 420, and 450–500 K. The remaining analyses will focus on four representative levels from these layers: 350 (near the core of the subtropical jet and a focus of many previous studies), 380 (coincident with previous tropospheric intrusion analyses), 420 (the observed peak in cyclonic wave-breaking events from Fig. 5), and 500 K (a level well into the tropical and extratropical stratosphere and near the altitude of the winter polar vortices).

Figure 7 shows the annual cycles of transport for both hemispheres stratified by wave-breaking sense and by transport direction. The Southern Hemisphere is shifted by 6 months to simplify comparisons between the hemispheres. The thick black line is the net transport from all components. As in Fig. 6, negative values represent equatorward transport.

At 350, 380, and 500 K, cyclonic wave breaking contributes very little to the transport in either direction, which is consistent with the observed wave-breaking frequency in Fig. 5. The annual cycles of poleward

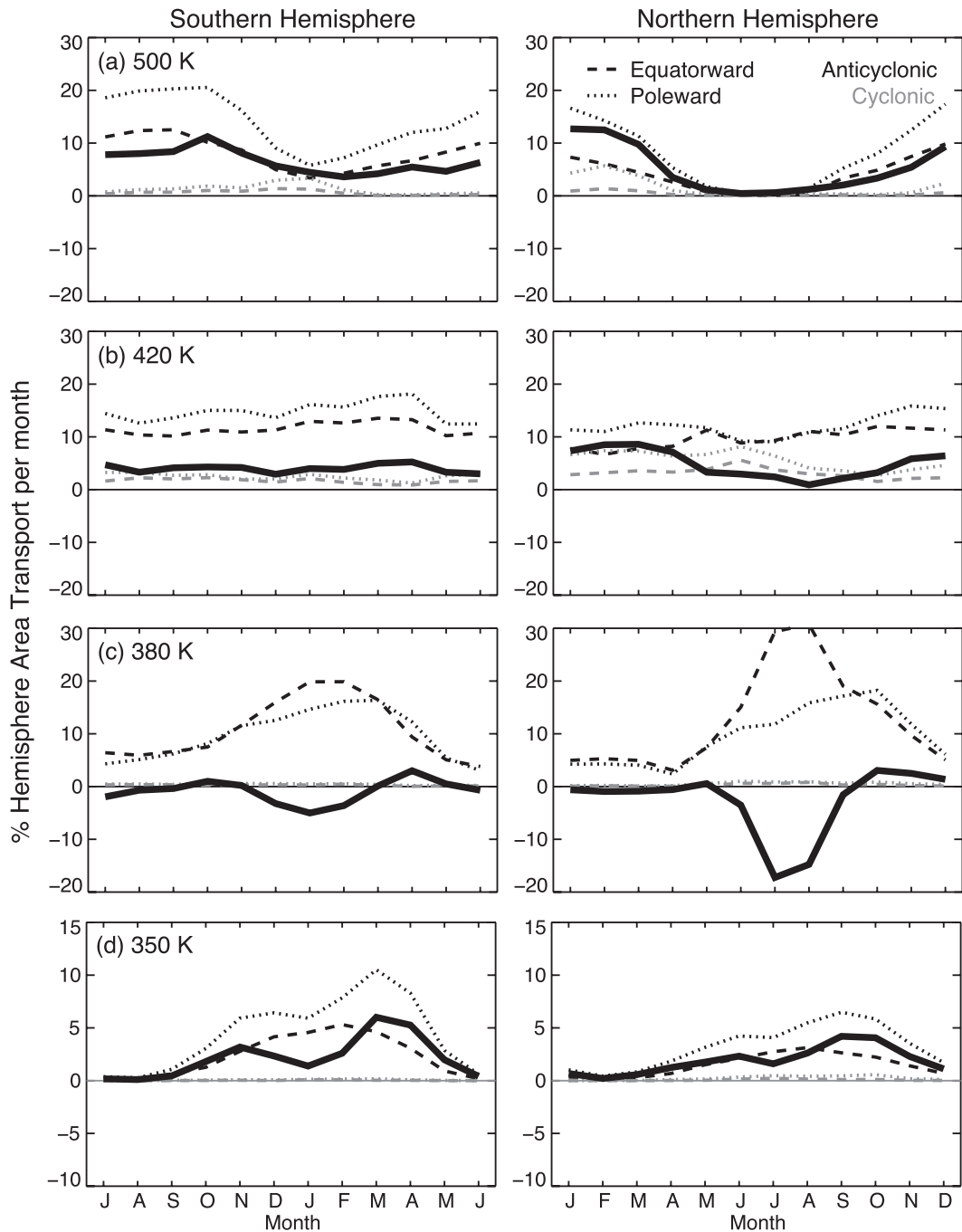


FIG. 7. Annual cycles of Rossby wave-breaking transport at (a) 500, (b) 420, (c) 380, and (d) 350 K. Anti-cyclonically sheared events are shown in black and cyclonically sheared events in gray. Dashed lines are equatorward transport and dotted lines poleward. The thick black line is the net transport, with negative values representing equatorward transport (stratosphere to troposphere at lower levels). Note that the abscissa is shifted 6 months between the two hemispheres and that the ordinate is doubly exaggerated for the panels at 350 K. Transport magnitudes are shown as the percentage of the area of one hemisphere.

transport at 350 and 380 K (dotted lines) have a fall maximum in both hemispheres, whereas equatorward transport reaches a maximum during each hemisphere's summer (dashed lines). At 350 K the net transport is

dominated by the poleward component. At 380 K the summer peak in equatorward transport exceeds the poleward component, leading to net equatorward transport. The maximum exchanges reach as high as 20%–30%

of the hemispheric area per month. During the remainder of the year at that level, the two components nearly cancel, with little net transport.

There is little annual cycle in either transport direction at 420 K, although there is a weak annual cycle in net transport with a spring maximum in the Northern Hemisphere. At 500 K, the annual cycles for both transport directions reach a maximum in both hemispheres during winter and spring, in agreement with the analysis of Waugh (1996). The transport magnitudes observed at 500 K in this analysis also agree with Waugh (1996), with the exception of the observed winter peak which is roughly twice the previously observed magnitude.

It is important to note that the near zero transport observed in both directions during winter at 350 K is likely due to our definition of transport in section 2c, which identifies only deep transport events ($\geq 5^\circ$ along-trajectory equivalent-latitude change over 10 days). There are wave-breaking events observed throughout the entire year at all levels, but transport and mixing is confined to a narrow region along the troposphere-stratosphere boundary during the annual minimum in wave-breaking frequency. Differences in seasonal and annual transport magnitudes between this study and previous studies may in part be a result of this definition.

As discussed in section 2b, PV at the tropopause break from the ERA-Interim is near ± 4 PVU in the 350–370-K potential temperature range while the ± 2 -PVU contour for troposphere–stratosphere separation used in previous studies lies deeper into the tropics. To test the dependence of transport magnitude and direction on the choice of PV contour, the same analysis techniques used for dynamical contours at the tropopause break are applied at 350 K using the ± 2 -PVU contour. Figure 8 shows the observed annual cycle of transport by hemisphere, wave-breaking sense, and transport direction. For both hemispheres, the net annual cycle of transport is now primarily equatorward (into the tropical troposphere), which is in agreement with previous studies. This analysis illustrates that the choice of troposphere-stratosphere boundary has a significant impact on the observed direction and magnitude of transport. This is especially true for surfaces that intersect the tropopause break at or below the tropical tropopause (e.g., 350–380 K), where meridional PV gradients are particularly sharp. The number of events identified along the ± 2 -PVU contour is slightly lower than at the tropopause break.

b. Geographical distributions

In addition to transport estimates of Rossby wave-breaking events, geographical distributions of wave-breaking events are useful for air mass source

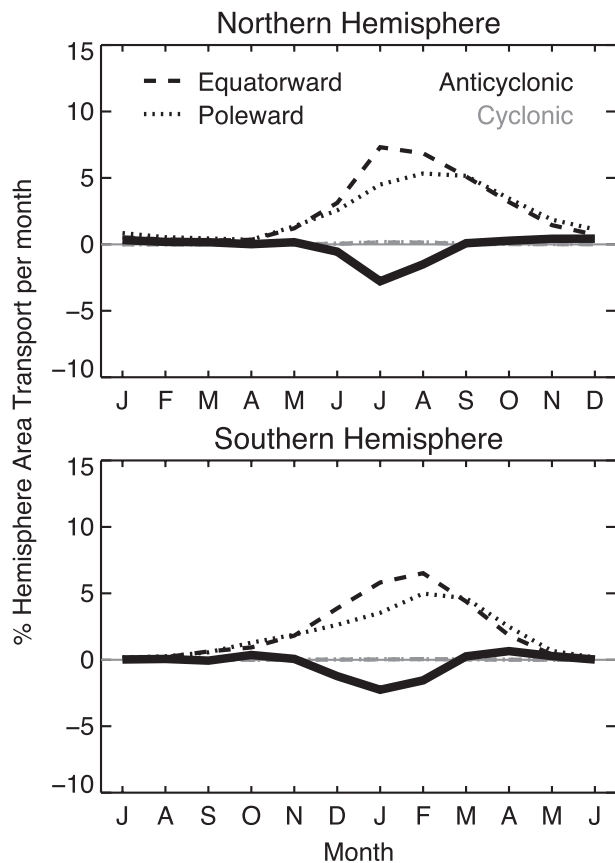


FIG. 8. As in Fig. 7d, but relative to the ± 2 -PVU contour of PV at 350 K.

characterization. Figure 9 shows hemispherically normalized geographical distributions of wave-breaking events for selected seasons and wave-breaking senses at the four potential temperature levels. The significant variations in the locations of wave-breaking maxima at different altitudes, especially in the Northern Hemisphere, illustrate the observed sensitivity of wave breaking to the mean flow. Wave breaking at lower altitudes is determined by the characteristics of the subtropical jet, while wave breaking aloft is largely controlled by the geometry of the polar vortices (e.g., Norton 1994; Waugh 1996). The transitional altitude between these competing flow regimes is near 420 K in the ERA-Interim (not shown).

Figure 9a shows the geographical distribution of anticyclonically sheared wave-breaking events at 350 K during each hemisphere's summer. In the Northern Hemisphere, two distinct maxima are observed: one over the central Pacific and another over the eastern Atlantic. In the Southern Hemisphere, one distinct maximum is observed in the southeastern Pacific just west of the southern tip of South America while a

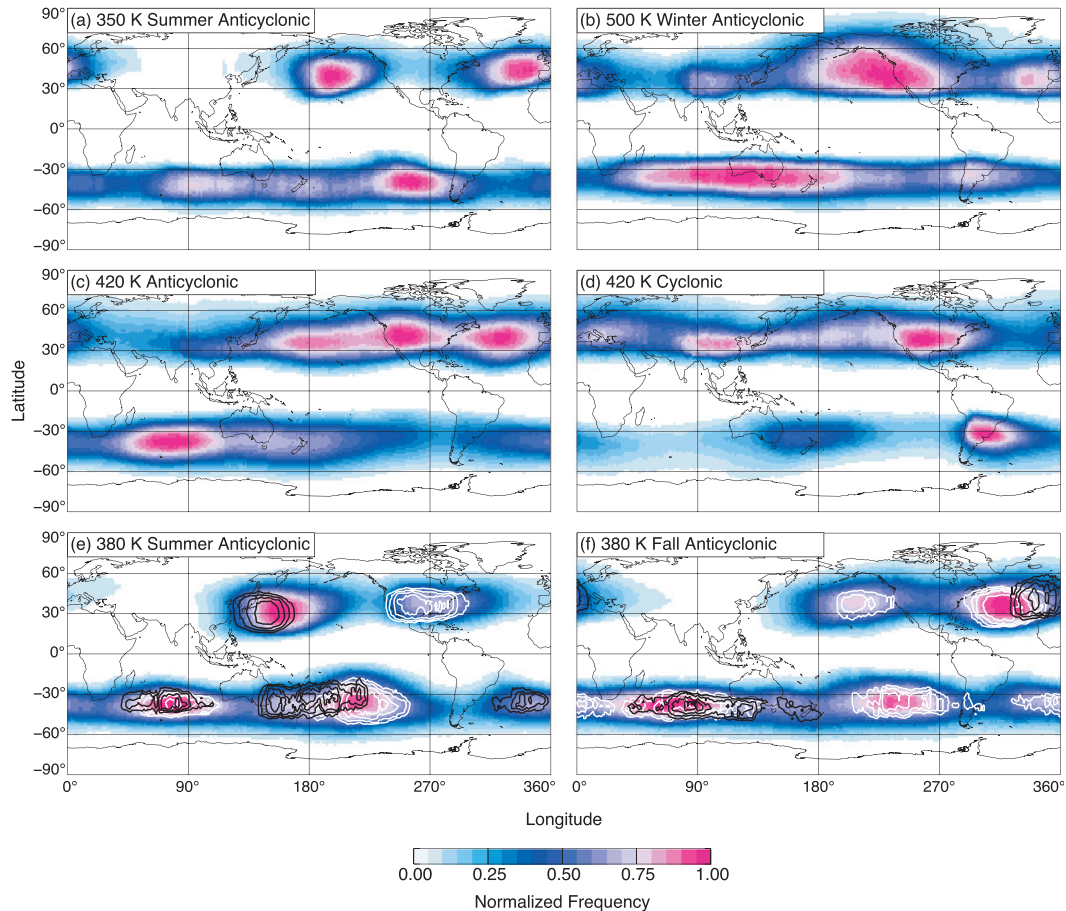


FIG. 9. Hemispherically normalized distributions of anticyclonically sheared wave-breaking events at (a) 350 K during summer, (b) 500 K during winter, and (c) 420 K during all seasons; (d) cyclonically sheared wave-breaking events at 420 K during all seasons; and anticyclonically sheared wave-breaking events at 380 K during (e) summer and (f) fall. The white contours in (e) and (f) represent normalized maxima of symmetric transport events and are contoured from 0.6 to 1.0 with an interval of 0.1. Similarly, the black contours in (e) represent predominantly equatorward transport events and in (f) predominantly poleward transport events. The transport designations correspond to the three frequency maxima identified in Fig. 10c.

Downloaded from http://journals.ametsoc.org/jas/article-pdf/70/2/607/2814304/jas-d-12-0198_1.pdf by guest on 28 October 2020

broader, less distinct maximum is observed south and west of Australia over the Indian Ocean. These distributions are comparable to previous climatologies at 350 K and are collocated with regions of weak westerlies (e.g., Postel and Hitchman 1999).

Figure 9b shows the geographical distribution of anticyclonic wave-breaking events at 500 K during each hemisphere's winter. This level is near the altitude of the polar vortices and above the vertical extent of the subtropical jet. One large, dominant maximum in wave-breaking frequency is observed in each hemisphere. The Northern Hemisphere maximum stretches from the south of Alaska to the south-central United States over the eastern Pacific. The Southern Hemisphere maximum, which is broader in longitude and narrower in latitude, stretches from the southeastern tip of Africa over the

Indian Ocean to the south-central Pacific. These results are qualitatively similar to those presented in Hitchman and Huesmann (2007).

Figures 9c and 9d show geographical distributions for all seasons at 420 K for anticyclonic and cyclonic wave-breaking events, respectively. The distribution of anticyclonic events at 420 K shows maxima consistent with features observed at 350 and 500 K and is evidence of contributions from wave breaking along the subtropical jet and wave breaking associated with the polar vortices. For cyclonically sheared wave-breaking events, maxima are found in regions of relatively low anticyclonic wave-breaking frequency and correspond to regions of equatorward displacements of the subtropical jet, which is in agreement with cyclonic meridional wind shear along the tropical boundary.

Figures 9e and 9f show geographical distributions of anticyclonic wave-breaking events at 380 K for the summer and fall, respectively. These two seasons are shown in order to characterize source regions of the three transport modes identified in Figs. 10, 11, and 12 in section 3c below. Overlaid on each map at 380 K are contours of hemispherically normalized frequency maxima of two of the three transport modes. The thick white contours in both maps show frequency maxima of the symmetric transport mode, which is a mode of comparable equatorward and poleward transport. In Fig. 9e (380 K, summer), the thick black contours show frequency maxima of predominately equatorward transport. Anticyclonic wave-breaking events that transport air deep into the tropics occur downstream of the quasi-stationary anticyclones in each hemisphere. In the Northern Hemisphere, the observed frequency maximum in the western Pacific is dominated by equatorward transport immediately downstream of the Southeast Asian monsoon anticyclone while the maximum over North America is dominated by symmetric transport. In the Southern Hemisphere, there are three maxima of equatorward transport. The maximum in the western Pacific is immediately downstream of the Australian monsoon anticyclone, while the maxima over the Indian Ocean and Atlantic are downstream of much smaller anticyclones that are not associated with the Australian monsoon. The maxima in equatorward transport over the Indian Ocean and southwestern Pacific are located upstream of symmetric transport maxima, while the weaker maximum over the southern Atlantic is dominated by equatorward transport.

In Fig. 9f (380 K, fall), the thick black contours show frequency maxima of predominately poleward transport. The maxima in wave-breaking frequency here occur in regions consistent with wave-breaking maxima at 350 K. In both hemispheres, poleward and symmetric transport frequency maxima are located within regions of weak climatological westerlies or “breaks” in the subtropical jet that are not associated with any stationary anticyclones (see Fig. 13 below). In addition, poleward transport frequency maxima lie immediately downstream and slightly poleward of symmetric transport frequency maxima in both hemispheres.

c. Mean flow characteristics

To address the questions raised in section 1 about the dependence of transport direction on the characteristics of the mean flow, we compute transport statistics of wave-breaking events stratified by the type of event. Figure 10 shows the joint frequency distributions of Rossby wave-breaking events as a function of f_i^P and f_i^E , defined in section 2c. Using fractional instead of absolute

areas helps to remove the effects of the size of wave-breaking events and focuses on the efficiency of irreversible transport in both directions. For cyclonically sheared wave-breaking events, transport is primarily poleward at all levels.

Three distinct modes of wave breaking with irreversible transport can be seen for anticyclonic events in Fig. 10. All three modes are visible at 380 K (Fig. 10c, gray arrows). A mode with predominately poleward transport (Fig. 10a) is evidenced by transport fractions of more than 70% of the tropical air mass and less than 15% of the extratropical air mass. Similarly, a mode with predominately equatorward transport (Fig. 10c) is evidenced by transport fractions of less than 15% of the tropical air mass and more than 70% of the extratropical air mass. Third, a mode with comparable transport in both directions (Fig. 10b) is evidenced by transport fractions of 30%–50% in each direction. The three frequency maxima are also observed at 420 K, but the equatorward mode is weak. The equatorward transport mode is not observed for the anticyclonic distributions at 350 or 500 K. The distributions in Fig. 10 are not separated by hemisphere because there is little difference between the hemispheres.

Using the three transport modes identified in Fig. 10c, composite mean dynamical fields from the ERA-Interim at the last identified time in each wave-breaking event life cycle are computed. Figure 11 shows composite mean equivalent latitude, wind speed and direction, and tropopause height of anticyclonic events at 380 K for each hemisphere for the poleward, equatorward, and symmetric transport modes. The number of events contributing to and the mean latitude of these composites are given in Table 1. For the poleward transport mode (Fig. 11a), the mean flow shows characteristics similar to that proposed in the introduction: a “split jet” where the subtropical jet on the upstream side of the breaking wave extends poleward and meridionally overlaps the equatorward branch of the subtropical jet on the downstream side [e.g., see Homeyer et al. (2011), their Fig. 5]. In the Northern Hemisphere, this split jet feature is clearly observed to have a large meridional overlap ($\sim 45^\circ$ of longitude). Although there is also evidence of distinct jet axes poleward and equatorward of the wave-breaking region in the Southern Hemisphere, the poleward jet axis stretches over the entire domain while the equatorward jet axis extends from the western edge of the wave-breaking signature ($\sim 15^\circ$ upstream) to approximately 35° downstream, approaching the latitude of the poleward subtropical jet.

For the equatorward transport mode (Fig. 11b), there is no evidence of a split subtropical jet in either hemisphere. There is, however, a weakening of the subtropical jet

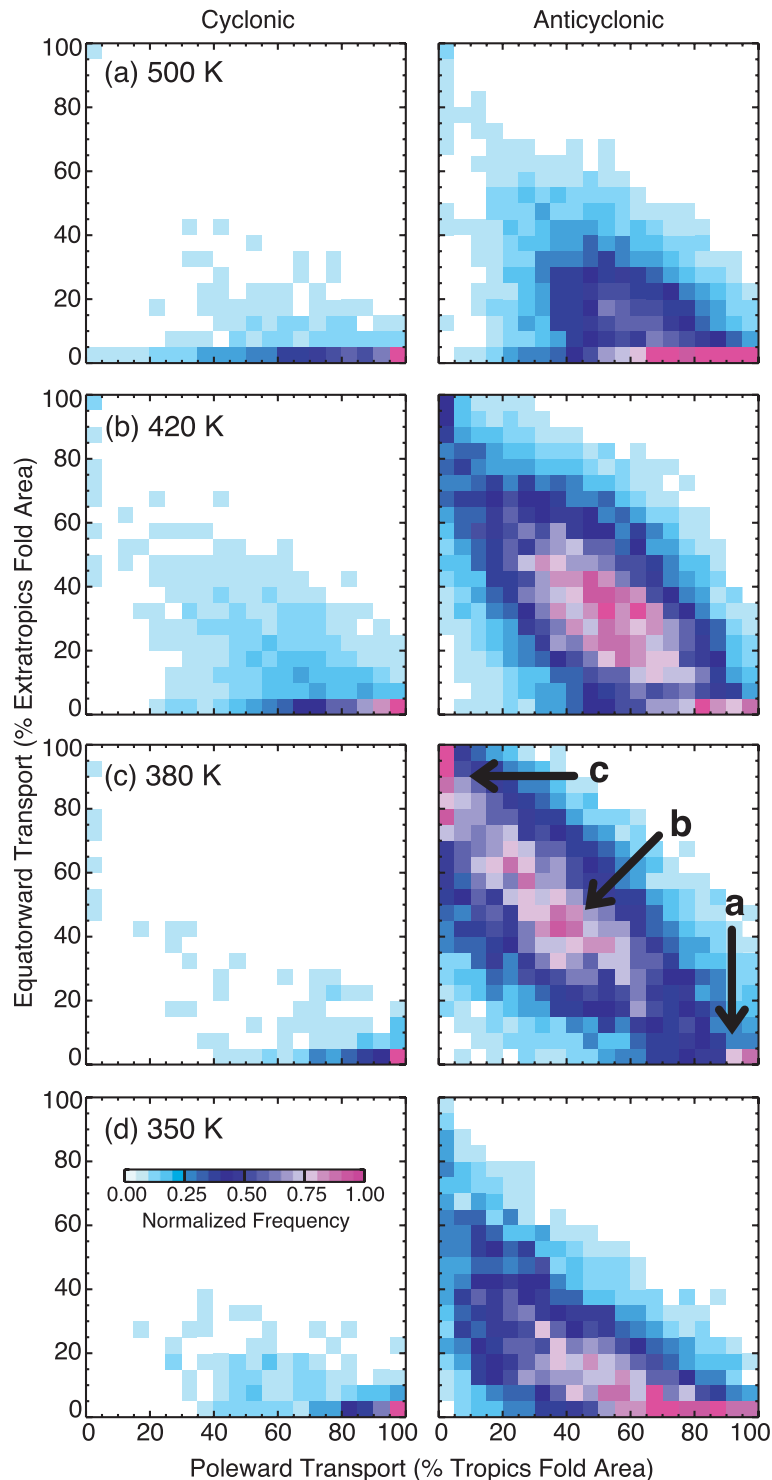


FIG. 10. Normalized joint frequency distributions of Rossby wave-breaking events as a function of poleward and equatorward transport fractions at (a) 500, (b) 420, (c) 380, and (d) 350 K for (left) cyclonically and (right) anticyclonically sheared events. Transport magnitudes are shown as the percentage of the analyzed area of each wave-breaking air mass. The arrows labeled "a," "b," and "c" for anticyclonically sheared events at 380 K correspond to frequency maxima in predominantly poleward, symmetric, and predominantly equatorward transport, respectively. These distributions were calculated using a bin resolution of $5\% \times 5\%$.

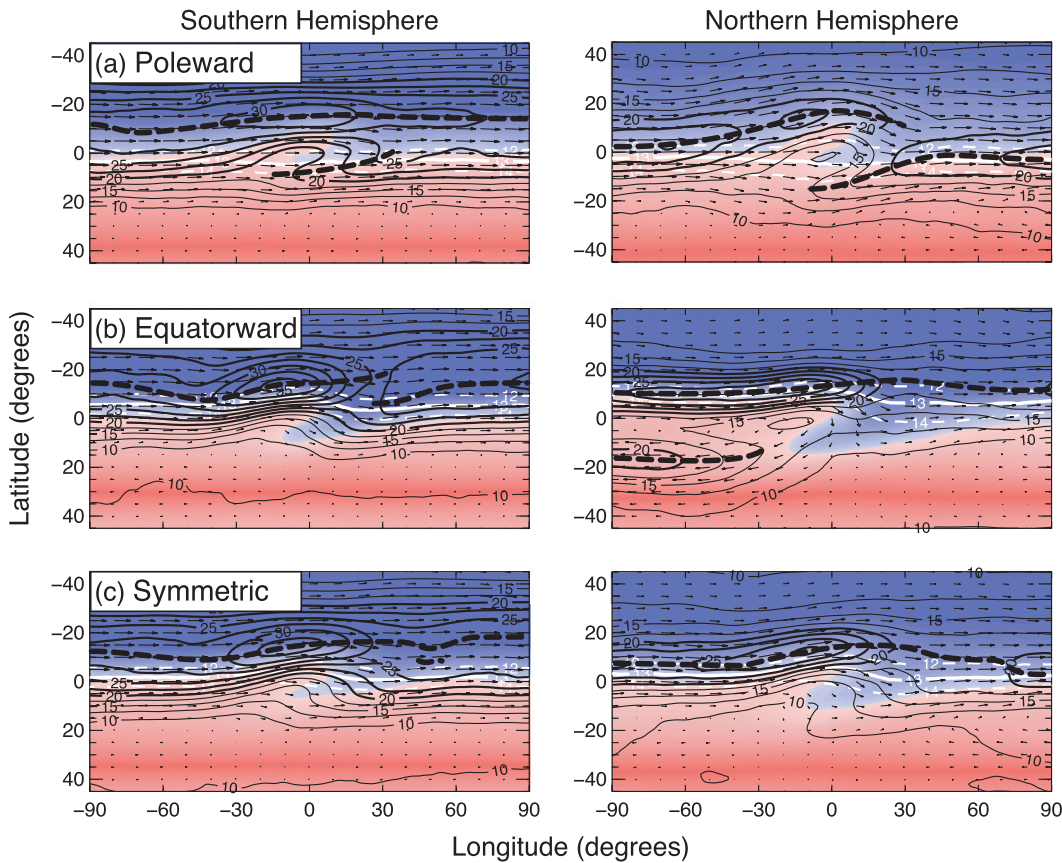


FIG. 11. Composite-mean equivalent latitude (color fill), wind speed (m s^{-1} , solid black lines), wind direction (vectors), jet axes (dashed black lines), and tropopause pressure altitudes of 12, 13 (solid), and 14 km (white lines) of anticyclonically sheared wave-breaking events on the 380-K potential temperature surface for (a) predominately poleward transport, (b) predominately equatorward transport, and (c) symmetric transport. The transport designations correspond to the three frequency maxima identified in Fig. 10c. Red colors of equivalent latitude represent air equatorward of the mean analyzed wave-breaking contour, while blue colors represent air poleward. Jet axes are shown as meridional maxima in wind speed for wind speeds exceeding 15 m s^{-1} . Note that the relative latitude axes for both hemispheres are oriented equator to pole. The number of events and their mean latitudes contributing to these composites are given in Table 1.

Downloaded from http://journals.ametsoc.org/jas/article-pdf/70/2/620/73814304/jas-d-12-0198_1.pdf by guest on 28 October 2020

immediately downstream of the breaking wave and a strong anticyclonic circulation upstream in the tropical reservoir of the Northern Hemisphere. In the Southern Hemisphere, there is also a slight weakening of the subtropical jet downstream of the breaking wave, evidenced by uncertainty in the location of the jet axis there. In addition, there is a much weaker anticyclonic circulation observed in the tropical reservoir upstream that is not clearly observed at the scale shown. The observed anticyclonic circulation upstream of the breaking wave in both hemispheres is in agreement with the geographical locations of these events discussed previously in section 3b (see Fig. 9e).

For the symmetric transport mode (Fig. 11c), the mean flow shows characteristics consistent with features of both directional modes, but with a nearly uniform

subtropical jet. The largest differences between hemispheres are observed downstream of the breaking wave, where the jet axis in the Northern Hemisphere tilts equatorward while the jet axis in the Southern Hemisphere tilts slightly poleward.

For these composite states, there are clear differences in the characteristic mean flow between hemispheres. The mean flow throughout the domain of each transport mode in the Southern Hemisphere is considerably stronger than in the Northern Hemisphere. The contrasting features between transport modes outlined above, however, are most distinct in the Northern Hemisphere. In addition, the meridional extent of the wave-breaking signature (equivalent-latitude fold) is smaller in the Southern Hemisphere for all modes, possibly because of the increased jet strength there. The observed

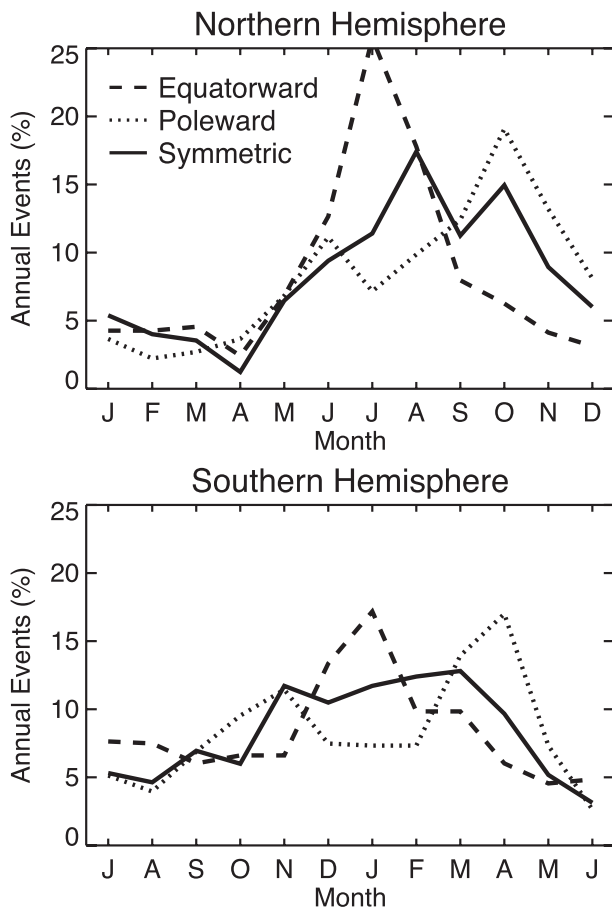


FIG. 12. Annual cycles of anticyclonically sheared wave-breaking events on the 380-K potential temperature surface for predominantly poleward transport (dotted lines), equatorward transport (dashed lines), and symmetric transport (solid lines). The transport designations correspond to the three frequency maxima identified in Fig. 10c. Note that the abscissa is shifted 6 months between the two hemispheres.

differences in flow geometry between hemispheres for the different transport modes may be related to differences in the large-scale geometry of the subtropical jet. In addition, the poleward and equatorward transport modes are consistent with the characteristics of primarily poleward (P2) and primarily equatorward (LC1) anticyclonic wave-breaking events, evidenced by the meridionally folded equivalent-latitude field relative to the mean 13-km tropopause altitude contour (the tropopause break) and the mean latitudes of the wave-breaking region (see Table 1).

Because the composites in Fig. 11 are computed late in the life cycles of the breaking waves, it is not clear whether the observed structures are characteristic of the mean flow in the absence of the wave, or simply indicative of the presence of the breaking waves themselves. To check this we computed composite mean states at

TABLE 1. Number and mean latitude $\bar{\phi}$ of wave-breaking events contributing to the transport-mode composites at 380 K in Fig. 11 for the Northern and Southern (in parentheses) Hemisphere.

	Poleward	Equatorward	Symmetric
No.	348 (494)	676 (659)	615 (706)
No. yr ⁻¹	11.6 (16.5)	22.5 (22.0)	20.5 (23.5)
$\bar{\phi}$	41.34°N (38.21°S)	30.72°N (30.06°S)	35.40°N (33.95°S)

earlier stages of the wave-breaking life cycles. These composites do not differ significantly from those at the end of the life cycles shown in Fig. 11. A split jet is observed at all identified times for poleward transport events. Similarly, a large upstream anticyclone is observed at all times for equatorward events. The most noticeable difference between earlier times in the life cycle and the composites shown in Fig. 11 is the scale of the equivalent-latitude fold, which elongates zonally throughout the wave-breaking life cycle, as would be expected from the evolution of the breaking wave. Differences in the mean wind speed and direction, as well as the location of the tropopause break, throughout the life cycle are small. Also, composite means for the identified transport modes at other levels dominated by the subtropical jet (i.e., below 420 K) are similar to Fig. 11 (not shown).

The seasonal dependency of the three transport modes illustrates their contribution to the observed annual cycle of transport at 380 K (Fig. 7c). Annual cycles of the monthly frequency of the three transport modes relative to the total annual frequency of each mode are shown in Fig. 12. For both hemispheres, the equatorward transport mode shows a distinct peak during summer while the poleward transport mode shows two peaks: a smaller one during late spring/early summer and one nearly twice as large during fall. Annual cycles of the symmetric transport mode show a broad peak from late spring to late fall in each hemisphere. These annual cycles in transport mode frequency illustrate that the directional transport modes largely control the observed annual cycles in the transport fractions in Fig. 7c. The annual cycles in transport show similar seasonality with less distinct peaks owing to the additional transport from symmetric events.

While equatorward anticyclonic wave-breaking events are shown to be dependent on strong, quasi-stationary anticyclonic circulations in both hemispheres, poleward and symmetric transport events depend on regional asymmetries in the subtropical jet that are not directly associated with these anticyclones. Previous studies have shown that wave breaking at 350 K, which we show to be dominated by poleward transport events, occurs in regions of weak climatological westerly winds. Figure 13 shows global climatological mean zonal wind speeds

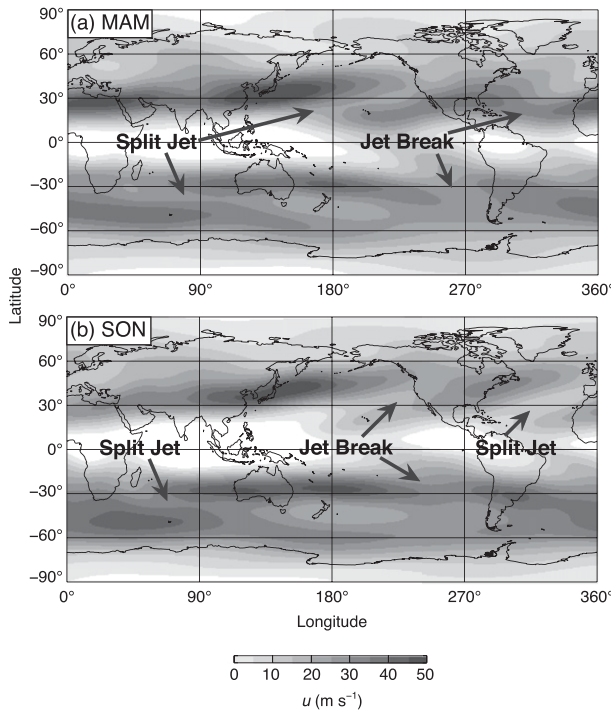


FIG. 13. Climatological mean zonal wind speed on the 350-K potential temperature surface from ERA-Interim during (a) MAM and (b) SON. White areas represent regions of climatological mean easterlies.

during the transition seasons at 350 K, which is near the core of the subtropical jet. During both transition seasons, climatological features consistent with the composite means for poleward and symmetric transport events can be seen in both hemispheres. Climatological split jets are most distinct during Northern Hemisphere spring [March–May (MAM)] over the central Pacific in the Northern Hemisphere and over the Indian Ocean in the Southern Hemisphere. In Northern Hemisphere fall [September–November (SON)], split-jet features are observed over the Atlantic in the Northern Hemisphere and again, over the Indian Ocean in the Southern Hemisphere. Comparison of these climatological features of the jet and the geographical distribution in Fig. 9f shows that poleward transport events occur within climatological split jets, which is in agreement with the composite means. Similarly, symmetric transport events occur both immediately upstream of split jets and near additional breaks in the subtropical jet. These associations suggest that the mean flow may not control the transport direction, and, of course, wave-breaking events may in turn affect the structure of the mean flow.

To test the impact of poleward wave-breaking events on the observed structure in the climatological mean flow, we compute mean winds with and without the

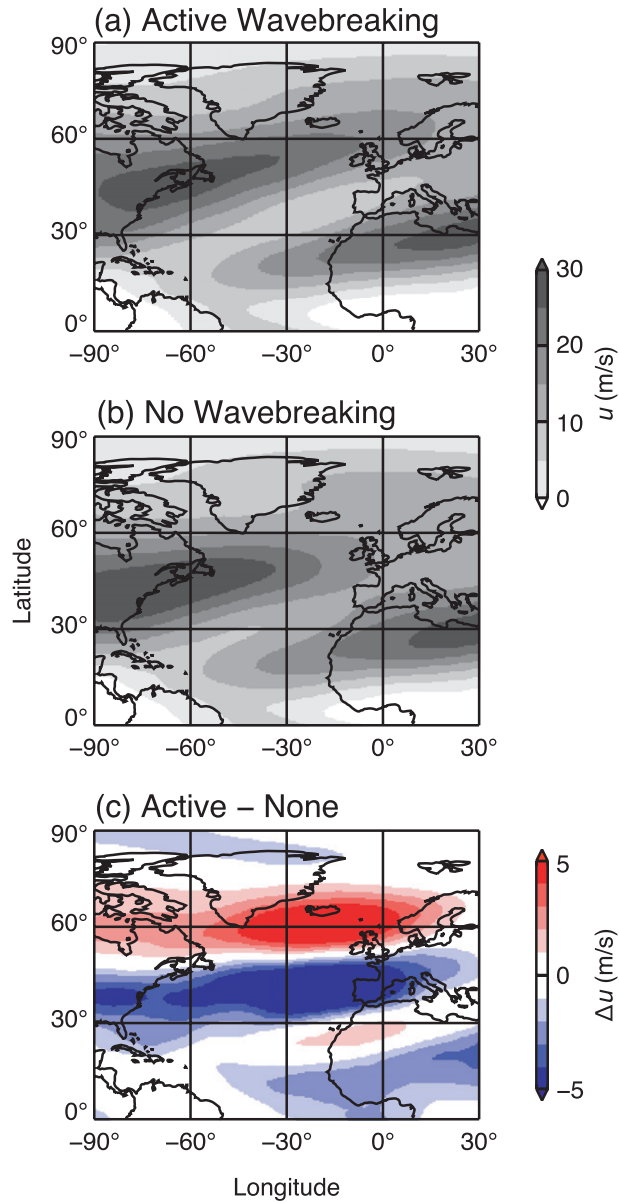


FIG. 14. Climatological mean zonal wind speed on the 350-K potential temperature surface from ERA-Interim during SON for analysis times with (a) active wave breaking within the domain, (b) no wave breaking, and (c) the difference (wave breaking – none).

actively breaking waves. Results are shown for the region of frequent poleward wave breaking over the northern Atlantic during North Hemisphere fall identified in Fig. 9f. Figures 14a and 14b show the mean zonal wind u for periods with and without breaking waves, respectively. Figure 14c shows the difference between wave-breaking and non-wave-breaking climatological means. These climatological means show that a split jet exists regardless of the presence of a breaking wave within the domain. The difference between the two

means shows that wave breaking results in a poleward shift of the upstream subtropical jet. These results suggest that the geometry of the mean flow near the location of the breaking wave determines the subsequent transport for all wave-breaking events. In addition, feedbacks may exist between the localization of wave breaking within the split-jet regions and the observed modulation of the split jet during wave-breaking events.

4. Summary and discussion

The observed frequency, seasonality, transport characteristics, and geographical distributions of Rossby wave-breaking events at the equivalent latitude of the tropopause break are analyzed in the 350–500-K potential temperature range using 30 yr of the ERA-Interim. Mesoscale motions that are not resolved by the 1.5° ERA Interim grid are not captured by this analysis. The results presented in this study are, with the exception of the transport direction, in good agreement with the results from previous studies of the “dynamical tropopause” at 350 K, which ranges from 1.5 to 3.5 PVU in the referenced literature. The observed seasonality and geographical distributions of wave-breaking events are consistent with that shown in previous studies, with a distinct peak during summer in each hemisphere. In this study, anticyclonically sheared wave-breaking events dominate in both hemispheres and at all altitudes, occurring most frequently in the Southern Hemisphere. Cyclonically sheared wave-breaking events are observed most frequently in the Northern Hemisphere and reach a maximum in the stratosphere at 420 K, strongly decreasing in frequency above and below this level in both hemispheres. Similarly, the total number of wave-breaking events reaches a maximum at 420 K, with the lowest wave-breaking frequencies observed near the core of the subtropical jet (350–360 K). Because wave breaking is shown to be associated with the characteristics of the jet, observed differences in the jet structures of the two hemispheres implies the observed differences in wave-breaking types.

Irreversible transport for each Rossby wave-breaking event was estimated using a Lagrangian method described in detail in section 2c. The net annual wave-breaking transport is observed to be equatorward within the 370–390-K potential temperature range and poleward at altitudes above and below. The observed differences between hemispheres in the depth of the net equatorward transport layer may be due to the vertical extent of associated anticyclonic circulations. Away from 420 K, transport from Rossby wave breaking shows significant seasonal variability with a strong peak during

hemisphere summer at lower levels (≤ 400 K) and a winter peak at upper levels (≥ 450 K), which is consistent with previous isentropic transport studies. Although the observed seasonal cycles in transport are consistent with results from previous work, the magnitude and direction of transport show significant differences. Notably, the observed direction of transport in the 350–360-K potential temperature range is in disagreement with previous studies. These discrepancies are shown to be largely dependent on the choice of tropics-extratropics (or troposphere-stratosphere) boundary in the dynamical field. Absolute values of PV at the tropopause break (or tropical boundary) in this study are found to be ≥ 4 PVU at all analyzed altitudes, while the more commonly used 2-PVU contour is found deeper into the tropics (Figs. 2b and 3a). When a PV value of ± 2 PVU is used for analysis, the transport direction is shown to reverse and become consistent with previous studies (contrast Figs. 7d and 8). The general characteristics of the geographical distributions at 350 K, however, seem to be independent of the analyzed dynamical boundary. As identified in section 2b, the annual cycle of a dynamical boundary at the tropopause can vary significantly and care should be taken when evaluating transport relative to such a boundary. Furthermore, several previous studies have also used ± 2 PVU as the troposphere-stratosphere boundary on lower potential temperature levels that vertically intersect the lapse-rate tropopause in the extratropics. Kunz et al. (2011) show that there is also significant seasonal variability in PV at the tropopause below 350 K, which is often nearer ± 3 PVU. The sensitivity of transport estimates to this boundary at lower levels is not known.

Frequency distributions of wave-breaking events as a function of the fractional transport of the tropical and extratropical air masses allow for the identification of three prevalent modes of anticyclonic wave-breaking transport near the subtropical jet: poleward, equatorward, and symmetric. Composite-mean meteorological and dynamical fields identify characteristics of the mean flow for each transport mode. The poleward transport mode is shown to be associated with a split subtropical jet, as proposed in the introduction and illustrated previously in individual case studies (e.g., Peters and Waugh 2003). Comparatively, events within the equatorward transport mode are shown to be located immediately downstream of large anticyclones during hemisphere summer and not associated with a split subtropical jet. These equatorward transport events are responsible for the observed net transport into the tropics in the 370–390-K potential temperature range and are primarily associated with monsoon circulations. Symmetric transport events are observed during all seasons and are generally

collocated with all global frequency maxima, except for that downstream of the Southeast Asian monsoon during North Hemisphere summer, which is uniquely a source for extratropics-to-tropics wave-breaking transport. Furthermore, the equatorward and poleward transport modes are comparable to the LC1 and P2 classifications from Thorncroft et al. (1993) and Peters and Waugh (1996), respectively.

The mechanisms for the development and maintenance of split subtropical jets are not known, though they occur frequently during transition seasons in both hemispheres (Fig. 13). Numerical studies suggest that their stability may, in part, be a result of baroclinic eddy accumulation poleward of a preexisting subtropical jet or eddy moment flux divergence between the poleward and equatorward jet components of a split jet (e.g., Lee and Kim 2003; Yoo and Lee 2010). The results presented here suggest that these splits in the subtropical jet are distinct pathways for tropical UTLS air into the extratropical LS during wave-breaking events. The characteristics of the mean state with or without wave breaking in these regions show only slight differences, suggesting that the geometry of the mean state in the region of wave breaking largely determines the subsequent transport (Fig. 14). Feedbacks between the localization of wave breaking within splits or breaks of the subtropical jet and modulation of these features by frequent Rossby wave breaking are potentially significant. Few studies have analyzed observations within these transported air masses and no in situ observations near the subtropical jet during the development of one of these wave-breaking events have been analyzed at this time. Additional studies are needed to develop an understanding of split-jet structures and any feedbacks related to Rossby wave breaking in these regions.

In addition, little is known about the dominant equatorward transport downstream of the monsoon circulations. Monsoon circulations are known to inject polluted boundary layer air deep into the tropical LS via convection and large-scale ascent (e.g., Randel et al. 2010). The results presented in this study suggest that transport of extratropical LS air into the tropics downstream of monsoon anticyclones may play a critical role in determining the composition of the tropical UTLS and subsequent ascent into the Brewer–Dobson circulation. In addition, recent analyses of satellite-retrieved ozone concentrations near the tropopause have revealed similar characteristics (e.g., Konopka et al. 2010; Ploeger et al. 2012). In situ meteorological and chemical observations of these processes will help to further characterize the climatological impact of these events. Additional analysis of trace-gas observations from satellites in the UTLS will also be helpful.

It is evident from the transport analyses presented and the example given in Fig. 1 that the sensitivity of transport to the dynamic boundary used, even between troposphere and stratosphere in the horizontal dimension, requires further evaluation. Previous studies have shown that the lapse-rate tropopause sharply identifies the transition between troposphere and stratosphere and tropics and extratropics, both chemically and dynamically (e.g., Pan et al. 2004; Hegglin et al. 2009; Gettelman et al. 2011). It has also been shown previously and within this study that dynamical variables such as PV (or equivalent latitude) at the lapse-rate tropopause can vary significantly with season and meteorological condition. Identifying the best representation of the boundary between troposphere and stratosphere in these dynamic variables at all altitudes is necessary for accurate transport determination. The use of a seasonally varying tropical boundary in this study shows that care must be taken when choosing the tropical–extratropical boundary in the 350–360-K potential temperature range. These results also suggest that commonly used nonvarying dynamic boundaries, such as 2 PVU, may not be the best representation of the boundary between troposphere and stratosphere above the subtropical jet. Consequently, transport studies at lower altitudes should be updated to reflect potential dependencies of the magnitude and direction of transport on the choice of troposphere–stratosphere boundary.

Acknowledgments. We thank the European Centre for Medium-Range Weather Forecasting for providing the ERA-Interim data, which were obtained from the Research Data Archive (RDA) maintained by the Computational and Information Systems Laboratory (CISL) at the National Center for Atmospheric Research (NCAR). The original data are available from the RDA (<http://dss.ucar.edu>) in dataset number ds627.0. This research was funded by National Science Foundation Grant AGS-1016191 to Texas A&M University.

REFERENCES

- Baray, J. L., S. Baldy, R. D. Diab, and J. P. Cammas, 2003: Dynamical study of a tropical cut-off low over South Africa, and its impact on tropospheric ozone. *Atmos. Environ.*, **37**, 1475–1488, doi:10.1016/S1352-2310(02)00999-8.
Benedict, J. J., S. Lee, and S. B. Feldstein, 2004: Synoptic view of the North Atlantic Oscillation. *J. Atmos. Sci.*, **61**, 121–144.
Birner, T., 2010: Recent widening of the tropical belt from global tropopause statistics: Sensitivities. *J. Geophys. Res.*, **115**, D23109, doi:10.1029/2010JD014664.
Bowman, K. P., 1993: Large-scale isentropic mixing properties of the Antarctic polar vortex from analyzed winds. *J. Geophys. Res.*, **98** (D12), 23 013–23 027.

- , and G. D. Carrie, 2002: The mean-meridional transport circulation of the troposphere in an idealized GCM. *J. Atmos. Sci.*, **59**, 1502–1514.
- , L. L. Pan, T. Campos, and R. Gao, 2007: Observations of fine-scale transport structure in the upper troposphere from the High-performance Instrumented Airborne Platform for Environmental Research. *J. Geophys. Res.*, **112**, D18111, doi:10.1029/2007JD008685.
- Bradshaw, N. G., G. Vaughan, R. Busen, S. Garcelon, R. Jones, T. Gardiner, and J. Hacker, 2002: Tracer filamentation generated by small-scale Rossby wave breaking in the lower stratosphere. *J. Geophys. Res.*, **107**, 4689, doi:10.1029/2002JD002086.
- Butchart, N., and E. E. Remsberg, 1986: The area of the stratospheric polar vortex as a diagnostic for tracer transport on an isentropic surface. *J. Atmos. Sci.*, **43**, 1319–1339.
- Castanheira, J. M. and L. Gimeno, 2011: Association of double tropopause events with baroclinic waves. *J. Geophys. Res.*, **116**, D19113, doi:10.1029/2011JD016163.
- Chen, P., J. R. Holton, A. O'Neill, and R. Swinbank, 1994: Isentropic mass exchange between the tropics and extratropics in the stratosphere. *J. Atmos. Sci.*, **51**, 3006–3018.
- Dee, D. P., and Coauthors, 2011: The ERA-Interim reanalysis: Configuration and performance of the data assimilation system. *Quart. J. Roy. Meteor. Soc.*, **137**, 553–597, doi:10.1002/qj.828.
- Dethof, A., A. O'Neill, and J. Slingo, 2000: Quantification of the isentropic mass transport across the dynamical tropopause. *J. Geophys. Res.*, **105** (D10), 12 279–12 293.
- Esler, J. G., and P. H. Haynes, 1999: Baroclinic wave breaking and the internal variability of the tropospheric circulation. *J. Atmos. Sci.*, **56**, 4014–4031.
- Gabriel, A., and D. Peters, 2008: A diagnostic study of different types of Rossby wave breaking events in the northern extratropics. *J. Meteor. Soc. Japan*, **86**, 613–631.
- Gettelman, A., P. Hoor, L. L. Pan, W. J. Randel, M. I. Hegglin, and T. Birner, 2011: The extratropical upper troposphere and lower stratosphere. *Rev. Geophys.*, **49**, RG3003, doi:10.1029/2011RG000355.
- Hegglin, M. I., C. D. Boone, G. L. Manney, and K. A. Walker, 2009: A global view of the extratropical tropopause transition layer from Atmospheric Chemistry Experiment Fourier Transform Spectrometer O₃, H₂O, and CO. *J. Geophys. Res.*, **114**, D00B11, doi:10.1029/2008JD009984.
- Hitchman, M. H., and A. S. Huesmann, 2007: A seasonal climatology of Rossby wave breaking in the 320–2000-K layer. *J. Atmos. Sci.*, **64**, 1922–1940.
- Holton, J. R., P. H. Haynes, M. E. McIntyre, A. R. Douglass, and L. Pfister, 1995: Stratosphere-troposphere exchange. *Rev. Geophys.*, **33**, 403–439.
- Homeyer, C. R., K. P. Bowman, and L. L. Pan, 2010: Extratropical tropopause transition layer characteristics from high-resolution sounding data. *J. Geophys. Res.*, **115**, D13108, doi:10.1029/2009JD013664.
- , —, —, E. L. Atlas, R.-S. Gao, and T. L. Campos, 2011: Dynamical and chemical characteristics of tropospheric intrusions observed during START08. *J. Geophys. Res.*, **116**, D06111, doi:10.1029/2010JD015098.
- Hudson, R. D., A. D. Frolov, M. F. Andrade, and M. B. Follette, 2003: The total ozone field separated into meteorological regimes. Part I: Defining the regimes. *J. Atmos. Sci.*, **60**, 1669–1677.
- Jing, P., D. M. Cunnold, E.-S. Yang, and H.-J. Wang, 2005: Influence of isentropic transport on seasonal ozone variations in the lower stratosphere and subtropical upper troposphere. *J. Geophys. Res.*, **110**, D10110, doi:10.1029/2004JD005416.
- Konopka, P., J.-U. Grob, G. Günther, F. Ploeger, R. Pommrich, R. Müller, and N. Livesey, 2010: Annual cycle of ozone at and above the tropical tropopause: Observations versus simulations with the Chemical Lagrangian Model of the Stratosphere (CLaMS). *Atmos. Chem. Phys.*, **10**, 121–132.
- Kunz, A., P. Konopka, R. Müller, and L. L. Pan, 2011: Dynamical tropopause based on isentropic potential vorticity gradients. *J. Geophys. Res.*, **116**, D01110, doi:10.1029/2010JD014343.
- Lee, S., and H.-K. Kim, 2003: The dynamical relationship between subtropical and eddy-driven jets. *J. Atmos. Sci.*, **60**, 1490–1503.
- Martius, O., C. Schwierz, and H. C. Davies, 2007: Breaking waves at the tropopause in the wintertime northern hemisphere: Climatological analyses of the orientation and the theoretical LC1/2 classification. *J. Atmos. Sci.*, **64**, 2576–2592.
- Matthews, A. J., and G. N. Kiladis, 2000: A model of Rossby waves linked to submonthly convection over the eastern tropical pacific. *J. Atmos. Sci.*, **57**, 3785–3798.
- McIntyre, M. E., and T. N. Palmer, 1983: Breaking planetary waves in the stratosphere. *Nature*, **305**, 593–600.
- Nakamura, M., and R. A. Plumb, 1994: The effects of flow asymmetry on the direction of Rossby wave breaking. *J. Atmos. Sci.*, **51**, 2031–2045.
- Nakamura, N., 2007: Extratropical stratosphere-troposphere mass exchange associated with isentropic mixing: A 1992–2005 climatology derived from advection-diffusion calculations. *J. Geophys. Res.*, **112**, D24303, doi:10.1029/2006JD008382.
- Ndarana, T., and D. W. Waugh, 2011: A climatology of Rossby wave breaking along the Southern Hemisphere tropopause. *J. Atmos. Sci.*, **68**, 798–811.
- Newman, P. A., and M. R. Schoeberl, 1995: A reinterpretation of the data from the NASA Stratosphere-Troposphere Exchange Project. *Geophys. Res. Lett.*, **22**, 2501–2504.
- Norton, W. A., 1994: Breaking Rossby waves in a model stratosphere diagnosed by a vortex-following coordinate system and a technique for advecting material contours. *J. Atmos. Sci.*, **51**, 654–673.
- O'Connor, F. M., G. Vaughan, and H. De Backer, 1999: Observations of subtropical air in the European mid-latitude lower stratosphere. *Quart. J. Roy. Meteor. Soc.*, **125**, 2965–2986.
- Pan, L. L. and L. A. Munchak, 2011: The relationship of cloud top to the tropopause and jet structure from CALIPSO data. *J. Geophys. Res.*, **116**, D12201, doi:10.1029/2010JD015462.
- , W. J. Randel, B. L. Gary, M. J. Mahoney, and E. J. Hintsa, 2004: Definitions and sharpness of the extratropical tropopause: A trace gas perspective. *J. Geophys. Res.*, **109**, D23103, doi:10.1029/2004JD004982.
- , and Coauthors, 2009: Tropospheric intrusions associated with the secondary tropopause. *J. Geophys. Res.*, **114**, D10302, doi:10.1029/2008JD011374.
- Pelly, J. L., and B. J. Hoskins, 2003: A new perspective on blocking. *J. Atmos. Sci.*, **60**, 743–755.
- Peters, D., and D. W. Waugh, 1996: Influence of barotropic shear on the poleward advection of upper-tropospheric air. *J. Atmos. Sci.*, **53**, 3013–3031.
- , and —, 2003: Rossby wave breaking in the Southern Hemisphere wintertime upper troposphere. *Mon. Wea. Rev.*, **131**, 2623–2634.
- Ploeger, F., and Coauthors, 2012: Horizontal transport affecting trace gas seasonality in the Tropical Tropopause Layer (TTL). *J. Geophys. Res.*, **117**, D09303, doi:10.1029/2011JD017267.

- Postel, G. A., and M. H. Hitchman, 1999: A climatology of Rossby wave breaking along the subtropical tropopause. *J. Atmos. Sci.*, **56**, 359–373.
- Randel, W. J., D. J. Seidel, and L. L. Pan, 2007: Observational characteristics of double tropauses. *J. Geophys. Res.*, **112**, D07309, doi:10.1029/2006JD007904.
- , M. Park, L. Emmons, D. Kinnison, P. Bernath, K. A. Walker, C. Boone, and H. Pumphrey, 2010: Asian monsoon transport of pollution to the stratosphere. *Science*, **328**, 611–613.
- Scott, R. K., and J.-P. Cammas, 2002: Wave breaking and mixing at the subtropical tropopause. *J. Atmos. Sci.*, **59**, 2347–2361.
- Seidel, D. J., and W. J. Randel, 2007: Recent widening of the tropical belt: Evidence from tropopause observations. *J. Geophys. Res.*, **112**, D20113, doi:10.1029/2007JD008861.
- Seo, K.-H., and K. P. Bowman, 2001: A climatology of isentropic cross-tropopause exchange. *J. Geophys. Res.*, **106** (D22), 28 159–28 172.
- Song, J., C. Li, J. Pan, and W. Zhou, 2011: Climatology of anticyclonic and cyclonic Rossby wave breaking on the dynamical tropopause in the Southern Hemisphere. *J. Climate*, **24**, 1239–1251.
- Thorncroft, C. D., B. J. Hoskins, and M. E. McIntyre, 1993: Two paradigms of baroclinic-wave life-cycle behaviour. *Quart. J. Roy. Meteor. Soc.*, **119**, 17–55.
- Vaughan, G., and C. Timmis, 1998: Transport of near-tropopause air into the lower midlatitude stratosphere. *Quart. J. Roy. Meteor. Soc.*, **124**, 1559–1578.
- Waugh, D. W., 1996: Seasonal variation of isentropic transport out of the tropical stratosphere. *J. Geophys. Res.*, **101** (D2), 4007–4023.
- , 2005: Impact of potential vorticity intrusions on subtropical upper tropospheric humidity. *J. Geophys. Res.*, **110**, D11305, doi:10.1029/2004JD005664.
- , and L. M. Polvani, 2000: Climatology of intrusions into the tropical upper troposphere. *Geophys. Res. Lett.*, **27**, 3857–3860.
- Wernli, H., and M. Sprenger, 2007: Identification and ERA-15 climatology of potential vorticity streamers and cutoffs near the extratropical tropopause. *J. Atmos. Sci.*, **64**, 1569–1586.
- World Meteorological Organization, 1957: Meteorology—A three-dimensional science: Second session of the commission for aerology. *WMO Bull.*, **4**, 134–138.
- Yoo, C., and S. Lee, 2010: Persistent multiple jets and PV staircase. *J. Atmos. Sci.*, **67**, 2279–2295.